# INTRODUCTION TO TIME-HARMONIC ANALYSIS OF POWER TRANSFORMERS WITH LAMINATED CORES USING THE ELECTROMAGNETIC FIELD SIMULATOR FINITE ELEMENT METHOD MAGNETICS

**Antônio Flavio Licarião Nogueira*, Leonardo José Amador Salas Maldonado, and Rodolfo Lauro Weinert**
Department of Electric Engineering, Santa Catarina State University, Joinville, Santa Catarina, Brazil
*Corresponding Author E-mail: antonioflavio.licariaonogueira@gmail.com

## ABSTRACT

Laminated magnetic materials may be treated as homogeneous anisotropic materials and this, overwhelmingly facilitates the numeric modeling of the laminated cores of transformers and electric machines. The bulk model implemented in the field simulator "finite element method magnetics" is based on the concept of effective permeability wherein the laminated structure is characterized by different permeabilities in the easy and hard direction of flux travel. The method used to compute the tensor of permeabilities varies according to the class of problem to be solved: magnetostatic, linear time-harmonic with thin laminations, linear time-harmonic with thick laminations, and nonlinear time-harmonic with thin laminations. The latter class of problem is used to simulate the no-load operation of the test transformer. Results are used to build the electric circuit of the energizing winding. This circuit is formed by frequency-dependent lumped elements that represent both, the core's magnetic loss and its magnetic stored energy. Two elementary applications of the electric circuit are used to check the self-consistency of output data. The discussion is supported by a parametric analysis that investigates the effect of hysteresis on the global quantities associated to the energizing winding. The main comparative study concerns the response of the energizing winding to increasing magnetic losses.

**Keywords**: *Eddy-current losses, Finite element analysis, Hysteresis, Magnetic losses, Transformer cores.*

## 1. INTRODUCTION

In two-dimensional (2-D) finite-element analysis, transformers are modeled as planar structures with stacked laminations parallel to the transverse (*x*-*y*) plane, as illustrated in Figure 1. This kind of structure with laminations parallel to the plane of analysis is commonly referred to as "laminated in plane". In 2-D finite-element analysis, driving and induced currents flow in the longitudinal or *z*-direction. Whenever the ferromagnetic core material is specified as a laminated structure, the analysis program implements an approximate bulk model for the core, based on the concept of effective permeability. Numerical modeling of magnetic losses in power transformers and electric machines is a very active area of research, and the accurate calculation of power losses in laminated cores still represents a major challenge in computational electromagnetics [1].

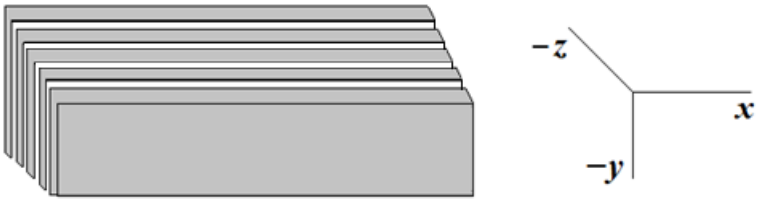


*Figure 1. I-shaped laminations parallel to the (x-y) plane.*

The study focuses on the computation of the electromagnetic quantities of power transformers with laminated cores using the nonlinear finite-element time-harmonic technique. Details of the test transformer's design including the relationship between the core's geometry and rated power, choice of windings and assembly of the laminated core are presented in [2]. A view of the test transformer showing details of the core's geometry appears in Figure 2.

In the test transformer, the coils are wound around the core's central limb, and the low-voltage circuit is wound over the top of the innermost high-voltage circuit. The windings are accommodated in the two rectangular windows with 13.6 mm width and 42.4 mm height each. The total number of turns of the high-voltage winding is $N_{HV}$=1100. Five series-connected windings with 30 turns each form the low-voltage circuit, so the total number of turns of the low-voltage winding is $N_{LV}$=150. The core is formed by M-36 steel laminations, and the stacking depth of the laminated core is 29 mm. Rated values of the test transformer are summarized in Table 1.

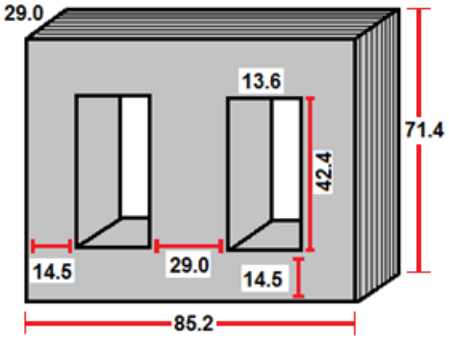


*Figure 2. View of the laminated core. Dimensions in mm.*

*Table 1. Rated values of the test transformer*

| Design parameter | High-voltage winding | Low-voltage winding |
|---|---|---|
| **Nº of turns** | 1100 | 150 |
| **Apparent power (VA)** | 58.0 | 58.0 |
| **RMS voltage (V)** | 220.0 | 30.0 |
| **RMS current (A)** | 0.26364 | 1.93333 |
| **Peak current (A)** | 0.37284 | 2.73415 |
| **Type of conductor** | 28 AWG | 24 AWG |

## 2. THE NONLINEAR TIME-HARMONIC TECHNIQUE

In the nonlinear time-harmonic (NTH) analysis, all excitations are sinusoidal, and it is assumed that the vector fields $\boldsymbol{H}$ and $\boldsymbol{B}$ are sinusoidal as well, but it considers the nonlinear relationship between the flux density and the magnetic field intensity [3]. The technique can be used to advantage whenever the excitations are sinusoidal, and only the steady-state solution is of interest [4], [5].

The concept of effective permeability forms the basis of numeric methods that incorporate the effects of eddy currents and hysteresis in the analysis of field problems subjected to cyclic magnetization. In these formulations, it is assumed that only quantities of a single time-harmonic exist, and the $\boldsymbol{B}$- and $\boldsymbol{H}$-fields are approximated by their fundamental components. The idea underlying these methods is to construct an apparent or effective $B_{\text{eff}}$-$H_{\text{eff}}$ characteristic based on a given criterion for the calculation of the complex-valued effective permeability.

The nonlinear time harmonic analysis implemented in the simulation software "finite element method magnetics" (FEMM) approximately models the effects of non-linearities like saturation and hysteresis on the fundamental component of the $\boldsymbol{B}$-field for different levels of the sinusoidal excitation represented by the $\boldsymbol{H}$-field. The amplitude of the fundamental component of the $\boldsymbol{B}$-field is obtained via Fourier analysis, and used to construct an apparent or effective $B_{\text{eff}}$-$H_{\text{eff}}$ characteristic. The nonlinear analysis is supported by two auxiliary data sets which represent the variations of both, the magnitude and phase of the complex effective permeability $\mu_{\text{eff}}$ with respect to the peak values of the exciting sinusoidal $\boldsymbol{H}$-field. The range of the field strength $\boldsymbol{H}_{\text{eff}}$ in the three effective characteristics is the same as the input set defined for the magnetostatic $B$-$H$ curve. Values of the magnetic induction, on the other hand, are adjusted yielding a curve with expanded range for $\boldsymbol{B}_{\text{eff}}$ wherein the magnetic induction values are typically higher than those defined by the $B$-$H$ input set.

## 3. THE BULK PERMEABILITY MODEL

In the bulk approach implemented in the simulation software "finite element method magnetics", the volume occupied by the laminations and adjacent insulating layers is treated as a homogeneous and anisotropic material [6]. The anisotropic material is characterized by two different permeabilities, defined according to the direction of flux travel: parallel to the lamination planes and across the lamination planes. When the magnetic flux travels parallel to the lamination planes, in the easy direction, the bulk permeability along this section of the magnetic circuit is given by

$$\mu_{easy} = c\mu_r\mu_0, \tag{1}$$

where $c$ is the fill factor of the pack of laminations, $\mu_r$ is the magnetostatic relative permeability, and $\mu_0$ is the permeability of free space. If the magnetic flux crosses the lamination planes perpendicularly, in the hard direction, the bulk permeability along this magnetic section is given by

$$\mu_{hard} = \frac{\mu_r\mu_0}{c + (1-c)\mu_r}. \tag{2}$$

The permeability tensor then takes the matrix form,

$$\vec{\mu} = \begin{bmatrix} \mu_{easy} & 0 \\ 0 & \mu_{hard} \end{bmatrix}. \tag{3}$$

The method used to compute the tensor of permeabilities $\boldsymbol{\mu}$ varies according to the class of problem to be solved. Four possibilities for the type of problem should be considered: (i) magnetostatic problems; (ii) linear time-harmonic problems involving thin laminations; (iii) linear time-harmonic problems involving thick laminations; and (iv) nonlinear time-harmonic problems involving thin laminations.

### 3.1. Magnetostatic problems

The permeabilities $\mu_{\text{easy}}$ and $\mu_{\text{hard}}$ are real-valued quantities, and are calculated by (1) and (2), respectively.

### 3.2. Thin laminations in linear time-harmonic problems

In magnetically linear time-harmonic problems involving thin laminations, the permeabilities are complex-valued quantities, and the calculation of the bulk permeabilities requires and additional step. This consists on the replacement in (1) and (2) of the magnetostatic permeability $\mu_r$ by the complex-valued and frequency-dependent effective permeability, $\mu_{\text{eff}}$, given by

$$\mu_{eff} = \frac{\mu_r e^{\frac{-j\phi_h}{2}} \tanh\left[\frac{-j\phi_h}{2}\sqrt{j\omega\sigma\mu_r\mu_0}\,\frac{d}{2}\right]}{\sqrt{j\omega\sigma\mu_r\mu_0}\,\frac{d}{2}}, \tag{4}$$

where $\phi_h$ represents a constant phase lag between the ***H***- and ***B***-fields, $\sigma$ is the electric conductivity of the lamination, $d$ is the thickness of the lamination, and $\omega$ is the angular frequency of excitation in rad/s. The effective permeability computed by (4) is then a function of the following parameters: (i) the depth of penetration $\delta$; (ii) the thickness of the lamination $d$; and (iii) the hysteresis lag angle $\phi_h$, so that

$$\mu_{eff} = \mu_{eff}(\delta, d, \phi_h). \tag{5}$$

It is important to observe that the dependence of the effective permeability with respect to the frequency of excitation and magnetostatic permeability is implicit in the definition of the depth of penetration,

$$\delta = \sqrt{\frac{2}{\omega\sigma\mu_r\mu_0}}. \tag{6}$$

The term "$\omega\sigma\mu_r\mu_0$" present on the RHS of (4) and (6) reveals that, the calculation of the effective permeability considers the skin effect, i.e., the attenuation of the ***H***-field below the surface of laminations due to the action of induced eddy currents.

The hysteresis lag angle $\phi_h$ that appears on the RHS of (4) is a user-defined parameter that must be specified together with the other physical properties that characterize a laminated core. This parameter is used in parametric analysis to determine the influence of hysteresis on the magnetic loss of electric machines and transformers as well as flux penetration in conductive media. The hysteresis angle must be determined experimentally, and different methods may be employed. Meeker [6] suggests an experimental set-up employing a frequency sweep on a toroidal coil with the core composed of the material of interest. Details of one experiment using a ring test circuit to obtain the frequency response are given by Meeker and Maslen [7]. A simple model for hysteresis in linear time-harmonic problems consists in approximating the hysteresis loop by an idealized elliptical characteristic. This model is described in [8], and has been incorporated in the assessment of hysteresis effects on: (i) flux penetration in conductive bodies [9]; and (ii) rotational losses in magnetic bearings [10]. This approximate hysteresis model ignores magnetic saturation as well as the difference between the minor and major hysteresis loops. The mathematical derivation of the method is presented in Appendix A.

### 3.3. Thin laminations in nonlinear time-harmonic problems

When the time-harmonic problem is magnetically nonlinear, the hysteresis lag angle becomes dependent on the effective permeability of the laminated core, and cannot be treated as a constant or fixed parameter. The phase lag between the ***B***- and ***H***-fields is now represented by a function of the exciting ***H***-field.

The definition of a nonlinear time-harmonic problem in the electromagnetic field simulator FEMM requires the set of input data illustrated in Figure 3. The special attributes of the lamination pack can easily be found in the built-in library or in the manufacturer's data sheets. As one can see in the illustration, in addition to the special attributes, the input data include: (i) the nonlinear *B*-*H* curve of the laminated material; and (ii) the specification of the "maximum" hysteresis angle $\phi_{hmax}$. The specification of this angle requires experience and judgment because there exists one hysteresis angle for each peak value of the exciting ***H***-field. As a consequence, the user-defined parameter $\phi_{hmax}$ represents a constraint on the value of the nonlinear curve that represents the variation of the hysteresis angle. The curve must be determined experimentally using several concentric hysteresis loops at different levels of excitation. The actual implementation of the nonlinear time-harmonic problem in the field simulator FEMM is based on the formulation initially proposed by O'Kelly [11], and followed by Jack and Mecrow [12]. A brief discussion on the method proposed by O'Kelly [11] is presented in Appendix B.

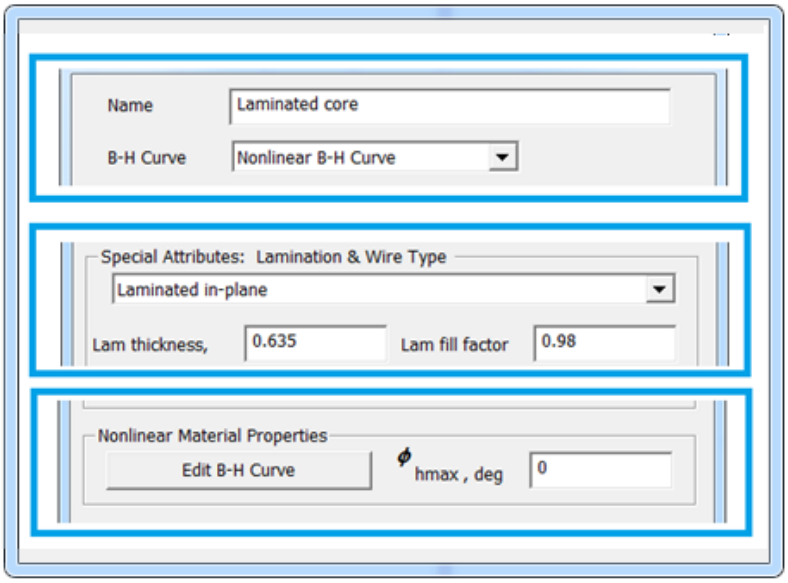


*Figure 3. Input data for a nonlinear time-harmonic problem.*

## 4. PROPERTIES OF LAMINATED CORES

In the following, it is presented a short description of the physical properties that characterize the laminated core of power transformers.

- ***B-H* data points**

This information is provided by an anhysteretic characteristic which can be obtained by different methods. Very often, manufacturers of soft material materials include in their data sheets the mean magnetization characteristic. To obtain this characteristic, the points at the first-quadrant tips of a family of concentric loops produced at different levels of excitation are joined to produce the mean magnetization curve [13]. In the sequence of simulations of the test transformer, M-36 steel laminations are employed in the ferromagnetic core. The *B*-*H* characteristic for this laminated material has been obtained from the field simulator's built-in library and is shown in Appendix C.

- **Electric conductivity**

Ideally, the conductivity of steel laminations should be very low, in order to further reduce eddy current loss. In practice, the reduction of eddy current loss in thin laminations is the result of two factors: (i) the low conductivity of the steel laminations; and (ii) the small thickness of the laminations. The electrical conductivity is part of the material properties of soft magnetic materials. For the M-36 steel, the conductivity is $\sigma_{M36}=2.0\text{x}10^6$ S/m.

- **Maximum hysteresis angle**

This parameter has a strong influence on the computed value of the magnetic loss. If the user-defined angle is zero, the hysteretic losses are not included, and the computed losses only include the effect of eddy currents. Typical data for low-loss, non-oriented grain steel sheet give a hysteresis angle of 30° for low flux densities ***B*** below the knee of the *B-H* curve, decreasing as the flux density goes into the saturated region [9]. For laminated steel structures, the hysteresis angle lies between 0° and 20° [6]. In our simulations, most of the results concern the original core configuration wherein the maximum hysteresis angle is specified as 20°.

- **Orientation of the pack of laminations**

The numeric model is based on the view of Figure 1 wherein the structure is "laminated in plane".

- **Thickness of individual laminations**

The laminated core is the main part of an electrical transformer, and accounts to approximately 70% of the transformer's cost. Transformer's steel laminations vary in thickness and "cold rolled grain oriented" (CRGO) laminations, for example, come in a thickness of 0.23 mm, 0.27 mm, 0.30 mm and 0.35 mm. In general, the lower the thickness of the lamination, the better is the quality of the laminated material. In the core of the test transformer, the thickness "*d*" of the M-36 steel laminations is $d_{M36}$=0.635 mm.

- **Fill factor of the stacked lamination**

This parameter represents the fraction of the core that is filled with laminations. A fill factor of 0.98 has been used in all simulations.

The physical properties of the M-36 steel laminations employed in the numerical simulations are summarized in the block scheme of Figure 4. This set of attributes and user-defined parameters for the M-36 pack of laminations will be referred to as the "original core configuration".

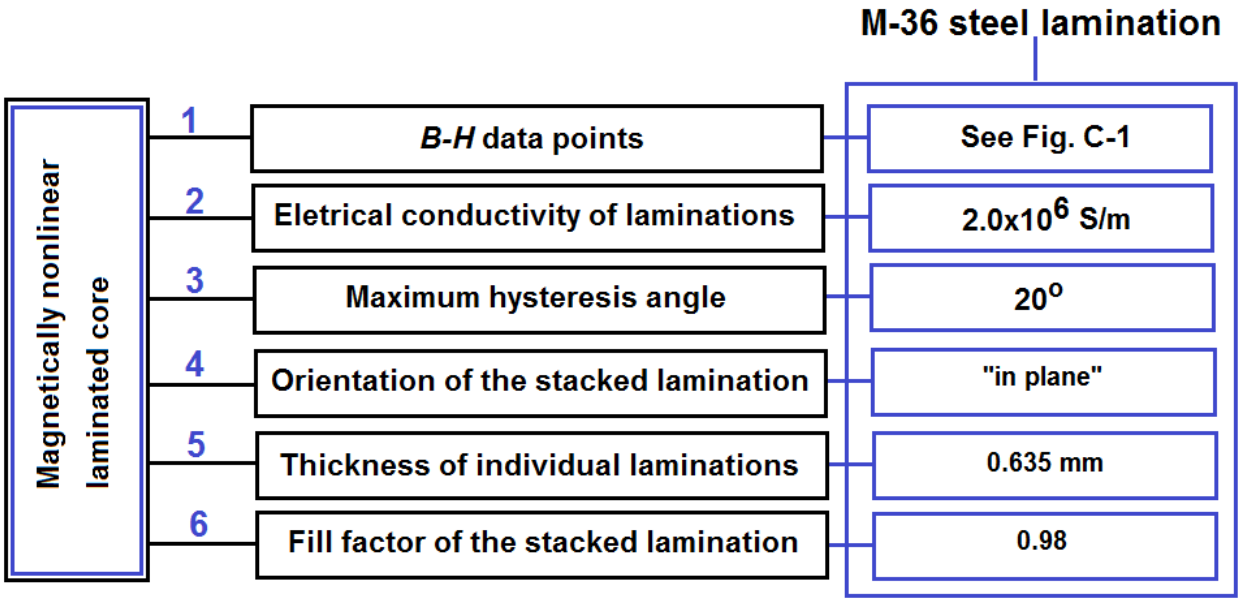


*Figure 4. Physical properties; original core configuration for the M-36 stacked lamination.*

## 5. FINITE ELEMENT SIMULATION

### 5.1. Features of the field simulator

The field simulator used in the work is a current-driven finite-element program that works with prescribed currents rather than voltages. In *AC* problems, the simulator always works with "peak" values, not root-mean square (*rms*) values. In this category of field simulators, the energy input of any modeled device is specified in terms of: (i) terminal currents; (ii) current densities in specific regions; and (iii) permanent magnets. The terminal voltage or voltage drop across a given winding is computed by the solver, rather than specified as input data.

In both *DC* and *AC* problems, the driving current is defined by its magnitude and its direction along the *z*-axis. By convention, a positive-valued current flows in the "out of page" direction whereas a negative-valued current flows in

the "into the page" direction. The driving current defined through "circuit properties" must be a positive or negative real-valued quantity. In static problems, the driving current can be defined indirectly, by choosing the option "source current density" and specifying the current density *J* in a given region.

### 5.2. Input data

#### 5.2.1. Driving current

In the main simulated experiment, the 1100-turn high-voltage winding is kept open-circuited, and the 150-turn low-voltage winding is supplied by a sinusoidal current of small magnitude at the frequency of 60-Hz. The exciting current in the low-voltage side represents 4.5% of the winding's rated current. As indicated in Table 1, the peak value of the rated current is 2.73415 A, so the excitation or driving current, expressed in terms of its peak value, is $\boldsymbol{I}$=123 mA.

To simulate the no-load operation of a two-winding transformer, it is necessary to define two "circuit properties", one for each winding. For the low-voltage winding, it is necessary to specify the exciting current, $\boldsymbol{I}$=123 mA, and the number of turns, $N_{LV}$=150. For the high-voltage winding, it is necessary to specify $\boldsymbol{I}$=0 for the winding's current and the number of turns, $N_{HV}$=1100. It is worth noting that a circuit property with total current $\boldsymbol{I}$=0 must be assigned to any winding kept open-circuited. This will enable the solver to compute the flux linkage with the open-circuited winding, as well as the related voltage drop. Values of flux linkages with all the windings are essential to any additional numeric computation of mutual inductances and analytical calculation of voltage drops.

#### 5.2.2. Laminated core configuration

The simulation of the transformer's no-load operation is based on the original core configuration, and the attributes for the laminated core formed by M-36 steel sheets are summarized in the block scheme of Figure 4.

### 5.3. Output data

Values of the electromagnetic quantities calculated by the simulation software for the low-voltage winding are summarized in Table 2. The high-voltage winding is kept open-circuited and only two of the electromagnetic quantities related to this winding are non-zero: the flux linkage and the voltage drop. These values are indicated in Table 3**.** It is worth noting that the complex numbers related to the currents, flux linkages and voltage drops indicated in Table 2 and Table 3 are the representations, in the frequency domain, of sinusoidally time-varying quantities. When these quantities are presented in polar coordinates, the magnitudes correspond to their peak values. These three quantities can also be treated as phasors in the frequency domain, this time with magnitudes expressed in "rms" values. The complex inductance and the inductive impedance indicated in the 4th and 5th lines of Table 2 are complex-valued quantities, not phasors.

*Table 2. Properties of the 150-turn low-voltage winding carrying a driving current* $\boldsymbol{I}$*=123 mA.*

| Order | Quantity (Unit) | Rectangular Coordinates | Polar Coordinates |
|---|---|---|---|
| **1** | **Total current (A)** | 0.123+j0.0 | 0.123 ∠0° |
| **2** | **Flux linkage (Wb)** | 0.0989337-j0.0552885 | 0.11333 ∠-29.3° |
| **3** | **Voltage drop (V)** | 20.9006+j37.2971 | 42.7540 ∠60.7° |
| **4** | **Complex inductance (H)** | 0.804339-j0.4495 | 0.92142 ∠-29.3° |
| **5** | **Ratio voltage/current (Ω)** | 169.4575+j303.22866 | 347.3665 ∠60.7° |
| **6** | **Complex power (VA)** | 1.28539 + j2.29377 | 2.62937 ∠60.7° |

The quantity referred to as "total current" that appears in the first line of Table 2 is also an input data. Its magnitude represents the peak value of the sinusoidal driving current in the energizing winding during the transformer's open-circuit operation. The flow of this relatively small current in the 150-turn winding creates an alternating magnetic flux that is linked with both windings. The peak value of the mutual flux is $\varphi_m$=0.755 milliweber.

#### 5.3.1. Flux linkage and voltage drop

The flux linkage with the 150-turn low-voltage winding is denoted by $\boldsymbol{\lambda}_{LV}$, and its value is indicated in the second line of Table 2. The flux linkage with the 1100-turn high-voltage winding is denoted by $\boldsymbol{\lambda}_{HV}$, and its value is indicated in the second line of Table 3**.** The magnitudes of the higher and lower flux linkages are $\|\boldsymbol{\lambda}_{HV}\|$ and $\|\boldsymbol{\lambda}_{LV}\|$, respectively. These magnitudes are related by the transformer's turns ratio,

$$\frac{\|\lambda_{HV}\|}{\|\lambda_{LV}\|} = \frac{N_{HV}}{N_{LV}} \cong 7.3 \tag{7}$$

The flux linkage $\boldsymbol{\lambda}_{LV}$ is used to compute the low-voltage winding's terminal voltage or "voltage drop" indicated in the third line of Table 2. In the same fashion, the flux linkage $\boldsymbol{\lambda}_{HV}$ is used to compute the high-voltage winding's terminal

voltage or "voltage drop" indicated in the third line of Table 3**.** The analytical calculation of voltage drops across the two windings using the flux-linkage method is presented in Appendix D.

*Table 3. Properties of the 1100-turn high-voltage winding at open-circuit operation.*

| Order | Quantity (Unit) | Rectangular Coordinates | Polar Coordinates |
|---|---|---|---|
| **1** | **Total current (A)** | 0.0+j0.0 | 0.0 ∠0° |
| **2** | **Flux linkage (Wb)** | -0.725436+j0.405449 | 0.8310 ∠150.7° |
| **3** | **Voltage drop (V)** | -152.851-j273.483 | 313.2992 ∠240.7° |

## 6. THE COMPLEX INDUCTANCE OF THE ENERGIZING WINDING

The lag of the flux linkage with respect to the driving current in a cored winding is caused by the combined effect of magnetic hysteresis and eddy currents. The relationship is illustrated in the phasor diagram of Figure 5. The flux linkage $\boldsymbol{\lambda}$ possesses a real component $\boldsymbol{\lambda}_r$ "in-phase" with the driving current $\boldsymbol{I}$ and an imaginary component $\boldsymbol{\lambda}_i$ that lags the driving current by 90°. It is worth noting that there is a strong difference between the specified maximum hysteresis angle $\phi_{hmax}$ and the angle $\theta$ that represents the phase lag of the flux linkage. The absolute value of $\theta$, the computed phase angle of the flux linkage, is always greater than the specified angle $\phi_{hmax}$. In this problem, for example, the value assigned to the maximum hysteresis angle $\phi_{hmax}$ is 20°. The angle $\theta$ that represents the phase lag of flux linkage $\boldsymbol{\lambda}$ with respect the driving current $\boldsymbol{I}$ has been computed as $\theta$= -29.3°, as one can see in the 2nd line of Table 2. The effect of an increasing hysteresis angle $\phi_{hmax}$ on global quantities like flux linkage, power loss and energy storage is discussed in Appendix E.

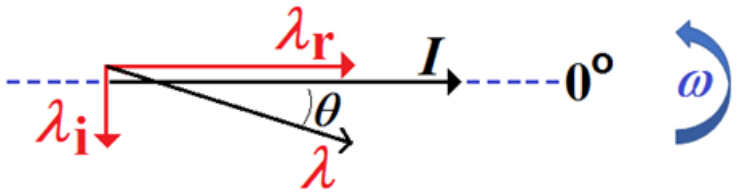


*Figure 5. Phasor diagram: phasor $\boldsymbol{\lambda}$ lags phasor $\boldsymbol{I}$.*

### 6.1. Complex inductance

If the winding's flux linkage and the driving current are represented by phasors (or rotating vectors) $\boldsymbol{\lambda}$ and $\boldsymbol{I}$, respectively, the complex-valued inductance $L$ can be defined by

$$L = \vec{\lambda} / \vec{I} \,. \tag{8}$$

The inductance $L$ can be decomposed as

$$L = L_r - jL_i \,, \tag{9}$$

where $L_r$ and $L_i$ are the real and imaginary components of $L$, respectively. Consider, now, the inductive impedance $Z$ that is implied,

$$Z = j\omega L, \tag{10}$$

where $\omega$ is the angular frequency of excitation. Substitution of the right-hand side of (9) into (10) leads to

$$Z = \omega L_i + j\omega L_r \,. \tag{11}$$

The inductive impedance of the energizing winding, $Z$, represents the lumped elements that form the series-connected circuit shown in Figure 6. In this circuit, $\boldsymbol{I}_S$ denotes the specified sinusoidal driving current, and $\boldsymbol{V}_S$ denotes the computed terminal voltage. A close observation of (9) and (11) shows that the imaginary part of the complex inductance contributes a real part to the inductive impedance, and is associated with losses. One could interpret the $\omega L_i$ term as the frequency-dependent part of the circuit's resistance. Higher values of the term $\omega L_i$ imply higher values of the active power $P$ drawn from the power supply. The real part of the complex inductance forms the imaginary part of the inductive impedance, and is associated with inductive energy storage. Lower values of the term $\omega L_r$ imply lower values of reactive power $Q$ flowing between the energy source and the winding.

The electric circuit that represents the no-load operation of the test transformer for the original core configuration is shown in Figure 6. The values of real and imaginary terms of the inductive impedance are indicated in the 5th line of Table 2. In this circuit, $\boldsymbol{I}_s$=0.123 ∠0° A represents the specified driving current and $\boldsymbol{V}_s$=42.75∠60.7° V represents the computed voltage, respectively. Once the magnitudes of $\boldsymbol{I}_s$ and $\boldsymbol{V}_s$ are expressed in peak values, the correspondent phasors $\boldsymbol{I}$ and $\boldsymbol{V}$, with magnitudes expressed in *rms* values are given by

$$\vec{I} = 0.123/\sqrt{2}\angle 0^\circ \text{ A}, \tag{12}$$

and

$$\vec{V} = 42.75/\sqrt{2}\angle 60.7^\circ \text{ V}, \tag{13}$$

respectively.

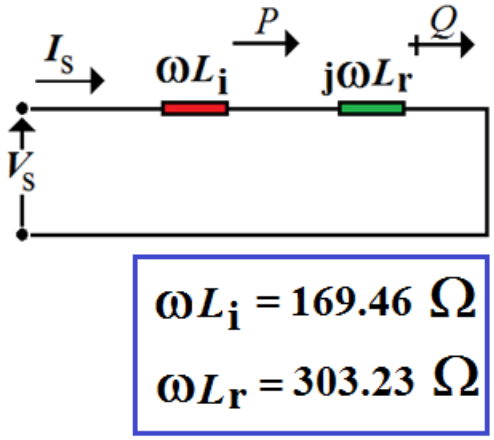


*Figure 6. Series-connected circuit for the energizing winding with frequency-dependent lumped elements.*

Two elementary applications of the circuit shown in Figure 6 are presented in Appendix F**.** The idea is to check the self-consistency of output data. The selected applications include: (i) the use of Kirchhoff's law of voltages; and (ii) the computation of complex power.

## 7. INDUCTIVE IMPEDANCE AND ITS RESPONSE TO INCREASING MAGNETIC LOSSES

Let us consider again the no-load operation of the test transformer with a 60 Hz driving current $\boldsymbol{I}_s$=0.123 mA supplying the low-voltage winding, and the numeric simulations for two different configurations of the magnetic core. The first configuration represents the hypothetical situation where a permeable but lossless magnetic core is used in the test transformer. To simulate the lossless core, the maximum hysteresis angle of the laminated material is specified as $\phi_{hmax}$=0° and the electric conductivity of the steel laminations is specified as $\sigma$=0. The second configuration represents a real situation where a permeable and lossy magnetic core is used in the test transformer. To eliminate the effect of magnetic hysteresis in the simulation of the lossy core, the maximum hysteresis angle is, once more, specified as $\phi_{hmax}$ =0°. To guarantee the presence of eddy currents in the magnetic core, the attributes of the M-36 steel laminations are assigned to the magnetically permeable core: (i) electric conductivity of $2.0\text{x}10^6$ S/m; (ii) thickness of 0.635 mm; (iii) and fill factor of 0.98. The *B*-*H* curve of the M-36 steel is employed in both simulations. The quantities of prime interest in the analysis are the active power *P*, the reactive power *Q*, the magnetic stored energy $W_m$, and the inductive impedance $Z=\omega L_i + j\omega L_r$. Results from the two simulations are summarized in Table 4.

*Table 4. Computed quantities for the two configurations of the laminated core.*

| **Quantity** | **Problem 1** | **Problem 2** |
|---|---|---|
| Active power, $P$ (W) | 0.00352717 | 0.56448 |
| Ratio $[P_2/P_1]$ (p.u.) | 160.04 | |
| Impedance, real component $\omega L_i$ ($\Omega$) | 0.46628 | 74.62220 |
| Ratio $[\omega L_{i2}/\omega L_{i1}]$ (p.u.) | 160.04 | |
| Reactive power, $Q$ (VAr) | 2.86459 | 2.72844 |
| Ratio $[Q_2/Q_1]$ (p.u.) | 0.952 | |
| Impedance, imaginary component $\omega L_r$ ($\Omega$) | 378.689 | 360.689 |
| Ratio $[\omega L_{r2}/\omega L_{r1}]$ (p.u.) | 0.952 | |
| Stored magnetic energy $W_m$ (mJ) | 3.79847 | 3.61790 |
| Ratio $[W_{m2}/W_{m1}]$ (p.u.) | 0.952 | |

When the transformer operates with a lossless core, only the ohmic loss in the winding conductor is present, and this small amount of loss is drawn from the supply. In the operation with a lossy core, the energy source must supply the winding's loss plus the ohmic loss in the magnetic core. With the aid of data presented in lines 1 and 2 of Table 4, one can observe that, in the second problem, the active power drawn from the power supply is 160.04 times greater than that of the first problem. It is worth noting that, the change into a lossy core configuration leads to the same ratio of increase in active power consumption and circuit's resistance, so that $(P_2/P_1)=[\omega L_{i2}/\omega L_{i1}]=160.04$ p.u.

In the operation with a lossless core, the flux-carrying capacity of the magnetic core is maximum and so is the energy stored in the core's magnetic field. In the operation with a lossy core, the eddy currents induced in the "metallic" laminations produce their own magnetic field that opposes the main field created by the "variation" of the driving current. This causes a reduction in the magnetic energy $W_m$ stored in the core and, in the same proportion, a decrease in the flow of reactive power $Q$ between the energy source and the winding. With the aid of data presented in lines 5 to 10 of Table 4 one observes that the change into a lossy core configuration yields a reduction of 4.8% in stored magnetic energy $W_m$ and, in the same proportion, a decrease in both, the flow of reactive power $Q$ and value of the inductive reactance $\omega L_r$.

## 8. CONCLUSIONS

The paper focuses on the nonlinear time-harmonic analysis of a small power transformer with M-36 steel laminated core. Initially, it examines the bulk permeability approach used to model thin laminations in time-harmonic problems. This is followed by a detailed description of the physical properties that characterize the laminated core of power transformers. The main test problem concerns the no-load operation of the test transformer for a given level of excitation and configuration of the magnetic core. It is presented a detailed description of the input data, and it is explained how to create circuit properties to model the transformer's windings. Values of the global quantities calculated by the simulation software are analyzed in detail. The computed global quantities include flux linkage, voltage drop and complex inductance. The value of the complex inductance is used to build an electric circuit with frequency-dependent lumped elements that represent the power loss and magnetic energy storage in the transformer's laminated core. Two elementary applications of the electric circuit are selected to check the self-consistency of output data. The overall discussion is supported by comparative studies and parametric analysis. The main comparative study concerns the response of the energizing winding to increasing magnetic losses. The main parametric analysis investigates the effect of hysteresis on global quantities like flux linkage, real power and reactive power.

## 9. ACKNOWLEDGEMENT

The authors acknowledge the financial support, in the form of scholarships, from the Brazilian Federal Agency for Postgraduate Studies (CAPES). They also wish to thank Dr. Airton Ramos (airton.ramos@udesc.br) for the use of the Laboratory of Applied Electromagnetism. The authors give thanks to David Meeker (dmeeker@ieee.org) for the use of the finite element CAD system. The authors also give thanks to Dr. Benedito Antonio Luciano (benedito@dee.ufcg.edu.br) for the useful comments on the manuscript.

## 10. REFERENCES


[1] H. Davtjan, J. Schöberl, M. Schöbinger, Karl Hollaus and M. Kaltenbacher, "Multiscale finite element methods for eddy current problems in laminated iron MSFEM4ECP", *International Compumag Society Newsletter*, Vol. 23, No 2, July 2016.

[2] A. Martignoni, Transformadores (Editora Globo, São Paulo, 8th ed., 2003) pp. 73.

[3] O. Bíró, G. Koczka and K. Preis, "TEAM problem No. 10 revisited: extension to sinusoidal voltage excitation", *International Compumag Society Newsletter*, Vol. 23, No 1, March 2016.

[4] J. D. Lavers, "Finite element solution of nonlinear two dimensional TE-mode eddy current problems", *IEEE Transactions on Magnetics*, Vol. MAG-19, No 5, pp. 2201-2203, 1983.

[5] G. Paoli and O. Bíró, "Complex representation in nonlinear time harmonic eddy current problems", *IEEE Transactions on Magnetics*, Vol. 34, No 5, pp. 2625-2628, 1998.

[6] Meeker, D.C. (2019) Finite Element Method Magnetics, User's Manual, Version 4.2., 2020. http://www.femm.info/wiki/HomePage

[7] D.C. Meeker and E.H. Maslen, "Prediction of rotating losses in heteropolar radial magnetic bearings", *Journal of Tribology*, 120(3):629-635, July 1998.

[8] R.L. Stoll, The Analysis of Eddy Currents (Oxford Univ. Press, London, 1974).

[9] D. O'Kelly, "Flux penetration in a ferromagnetic material including hysteresis and eddy-current effects", *J. Phys. D: Appl. Phys*., Vol. 5, pp. 203-213, 1972.

[10] D.C. Meeker, A.V. Filatov and E.H. Maslen, "Effect of magnetic hysteresis on rotational losses in heteropolar magnetic bearings, *IEEE Transactions on Magnetics*, Vol. 40, No 5, pp. 3302-3307, 2004.

[11] D. O'Kelly, "Hysteresis and eddy-current losses in steel plates with nonlinear magnetisation characteristics", *Proc. IEE*, Vol No 11, November 1972.

[12] A.G. Jack and B.C. Mecrow, "Methods for magnetically nonlinear problems involving significant hysteresis and eddy currents", *IEEE Transactions on Magnetics*, Vol. 26, No 2, pp. 424-429, 1990.

[13] G.R. Slemon and A. Straughen, *Electric machines* (Addison Wesley Publishing Company, London, 1982).


### Appendix A: Approximating the hysteresis loop by an idealized elliptical characteristic

The effect of hysteresis can be included in the analysis of linear time-harmonic problems by introducing a time phase difference between the ***B***- and ***H***-fields, defined as the hysteresis angle $\phi_h$ of the magnetic material. This situation is illustrated in the diagram shown in Figure A-1. In this model, the hysteresis loop becomes an ellipse with its major axis making an angle of $\phi_h$ radians with the *H*-axis. One can define the complex permeability due to hysteresis as

$$\mu_h = \frac{|B|}{|H|} e^{j(0-\phi_h)}, \tag{A.1}$$

and the complex permeability can be expressed in the usual form,

$$\mu_h = |\mu_h| e^{-j\phi_h}. \tag{A.2}$$

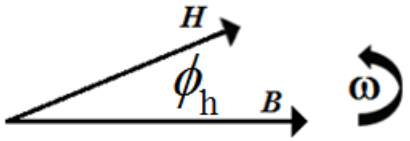


*Figure A-1. Phasor diagram: the B-field lags the H-field.*

The idealized hysteresis loops shown in Figure A-2 are used in the computation of the parameters $|\mu_h|$ and $\phi_h$ that appear on the RHS of (A.2). According to the illustration of Figure A-2(b), the angle $\alpha$ is computed by

$$\alpha = \tan^{-1}(w/l). \tag{A.3}$$

The major axis of the ellipse makes an angle $\phi_h=2\alpha$ with the *H*- axis. The angle $\phi_h$ represents the constant phase lag between the ***B***- and ***H***-fields, and is used to compute the magnitude of the complex permeability, $|\mu_h|$,

$$|\mu_h| = \tan^{-1}(\phi_h). \tag{A.4}$$

This approximate allowance for the effect of hysteresis leads to

$$B = \mu_h H, \tag{A.5}$$

where the complex permeability due to hysteresis $\mu_h$ is given by

$$\mu_h = \tan^{-1}(\phi_h) e^{-j\phi_h}. \tag{A.6}$$

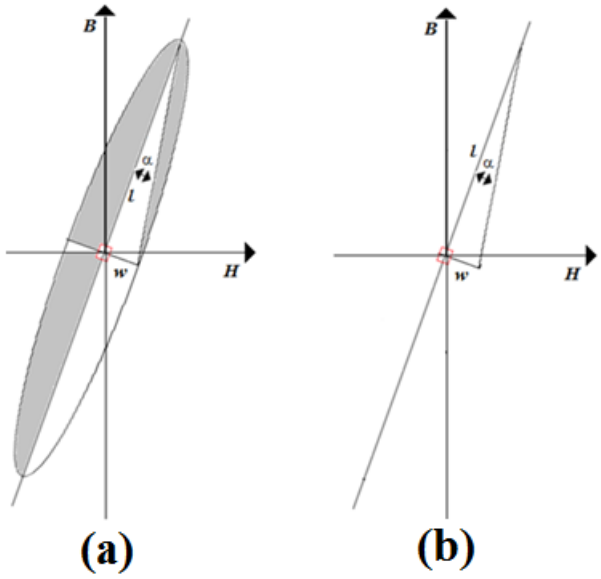


*Figure A-2. (a) Idealized hysteresis loop; (b) Geometric details.*

**Appendix B: Hysteresis angle and effective permeability in nonlinear time-harmonic problems**

When the time-harmonic problem is magnetically nonlinear, the hysteresis lag angle becomes dependent on the effective permeability of the laminated core. The method employed in the field simulator FEMM to compute "the "nonlinear hysteresis lag angle" is based on the formulation described by O'Kelly [11].

The method proposed by O'Kelly [11] involves the measurement of several hysteresis loops, one for each level of the exciting ***H***-field. If the energizing winding is supplied by a purely sinusoidal current, the ***H***-field is sinusoidal, but the ***B***-field is top-flatted and non-sinusoidal. Once all harmonic effects are to be neglected, only the fundamental component of the non-sinusoidal wave of the ***B***-field is used to determine the hysteresis angle $\delta_h$ related to a given loop. The simultaneous plot of the two time-varying characteristics representing the ***H***-field and the fundamental component of the ***B***-field permits to determine the phase lag between the two characteristics. The illustration of Figure B-1 represents the situation where the phase lag $\delta_h$ is 30°. The required steps to determine the pair of values ($\delta_h$, $B_p$) associated with one hysteresis loop are summarized in the block scheme of Figure B-2.

The value of the hysteresis angle and the peak value of the fundamental ***B***-characteristic, $B_p$, are now used to build the two auxiliary characteristics: (i) the hysteresis-angle characteristic; and (ii) the fundamental-magnetization characteristic. The independent variable of both characteristics is $H_p$, the peak value of the exciting ***H***-field. These two characteristics are illustrated in the graph of Figure B-3. At this stage, it is still necessary to adjust the values of $B_p$ to obtain the effective flux densities $B_{p,eff}$. This leads to a slight increase in the values of the flux densities.

The following step consists on the computation of the set of complex relative permeabilities. For each value of the independent variable $H_p$, the laminated material has a complex-valued relative permeability, $\mu_{eff}$, defined by:

$$\mu_{eff} = \frac{B_{p,eff}}{\mu_0 H_p} e^{-j\delta_h}. \tag{B.1}$$

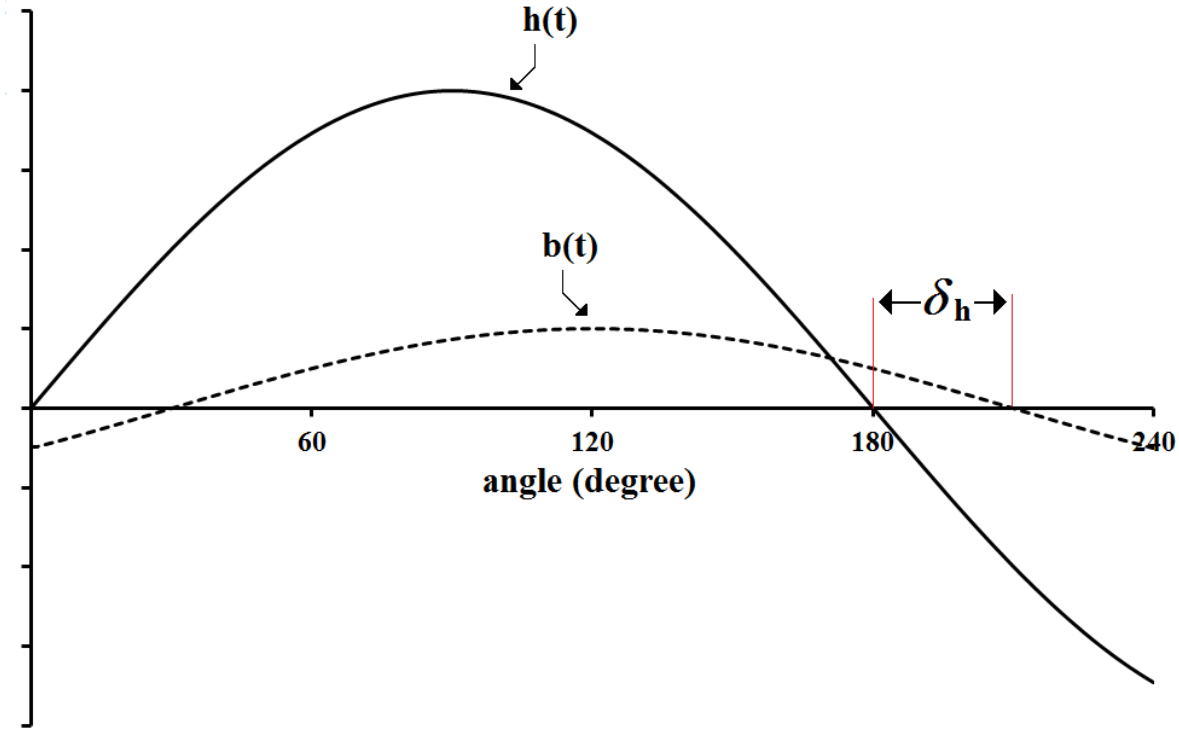


*Figure B-1. Phase lag of the fundamental component of the **B**-field.*

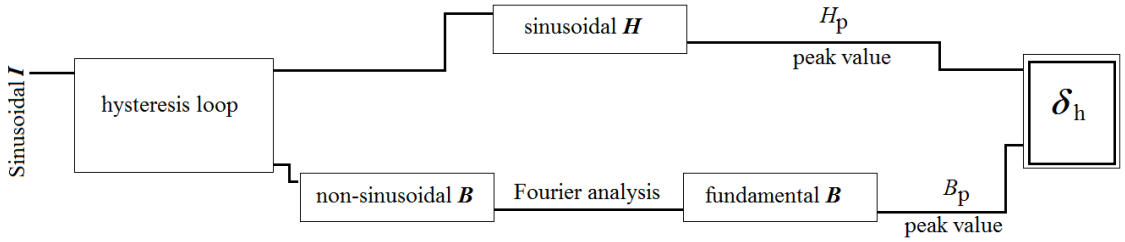


*Figure B-2: Required steps to built-up the complex-permeability auxiliary characteristics.*

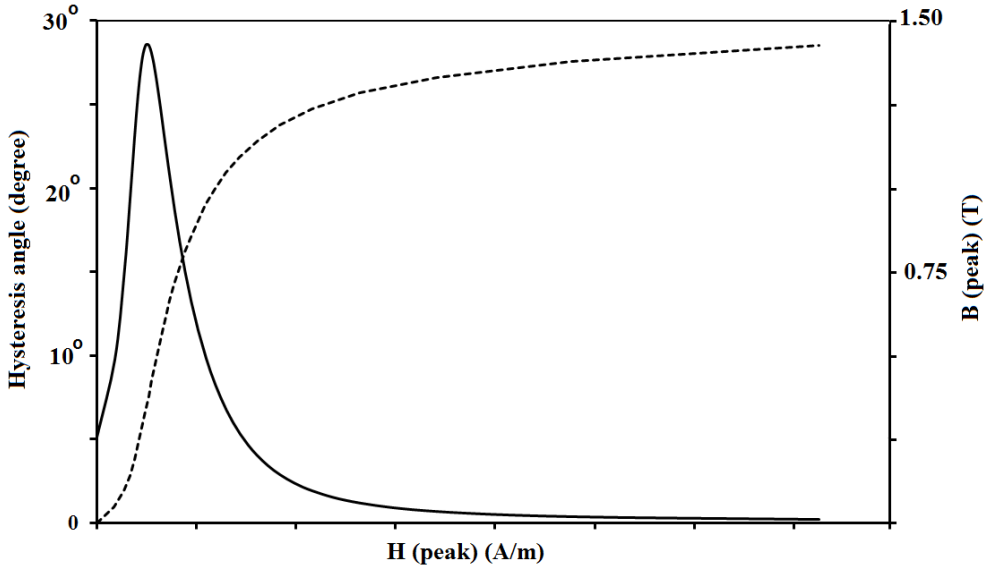


*Figure B-3. Complex-permeability auxiliary characteristics. Solid curve: hysteresis angle; dashed curve: fundamental-magnetization characteristic.*

**Appendix C: Magnetization characteristic for the M-36 steel**

The magnetization characteristic *B*=B(*H*) for the M-36 steel expressed as a 1st quadrant curve is shown in Figure C-1. The increments along the horizontal axis are 100.0 A/m between ticks, and the increments along the vertical axis are 0.2 T. Values of the magnetic induction *B* extend up to 1.50 T.

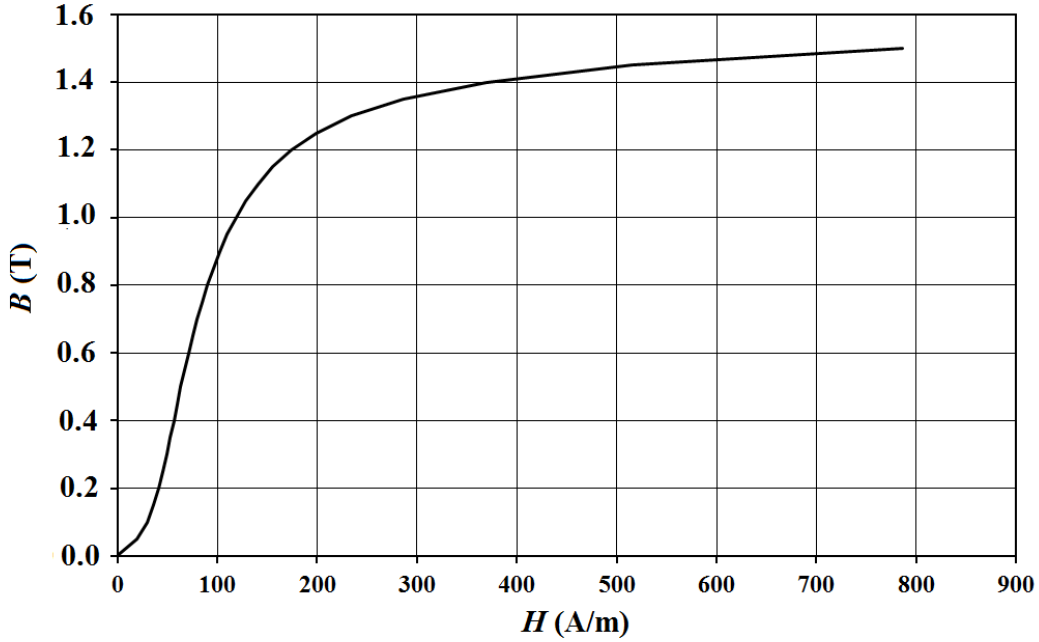


*Figure C-1. Magnetization curve for the M-36 steel.*

**Appendix D: Analytical calculation of voltage drop**

**Phasors and rotating vectors in the frequency domain**

The main difference between vectors and phasors is that the magnitude of a vector is equal to the "peak value" of the sinusoid, whereas the magnitude of a phasor is equal to the "rms" value of the sinusoid. In both cases, the phase angle and direction of a vector and related phasor are the same.

**Analytical calculation of voltage drop**

Let $\boldsymbol{\lambda}$ denote the rotating vector that represents the flux linkage with a given winding. According to Faraday's law of induction, the vector $\boldsymbol{V}$ that represents the voltage drop across the winding is calculated by

$$\vec{V} = j\omega\vec{\lambda}, \tag{D.1}$$

where $j\omega$ is the quadrature operator that replaces the time derivative *d*/dt of the time-varying formulation.

**Voltage drop in the low-voltage winding**

Let $\boldsymbol{\lambda}$ denote the rotating vector associated to the flux linkage with the low-voltage winding. The flux linkage $\boldsymbol{\lambda}$ can be decomposed in terms of its real and imaginary components,

$$\vec{\lambda} = \vec{\lambda}_r + j\vec{\lambda}_i, \tag{D.2}$$

where $\lambda_r$ and $\lambda_i$ are the real and imaginary components of vector $\boldsymbol{\lambda}$, respectively. The expression for the voltage drop $\boldsymbol{V}$ can be recast in terms of real and imaginary components. Substitution of the right-hand side of (D.2) into (D.1), gives

$$\vec{V} = -\omega\lambda_i + j\omega\lambda_r. \tag{D.3}$$

According to the numeric values indicated in the second line of Table 2, the real and imaginary parts of the flux linkage with the low-voltage winding are $\lambda_r$=0.0989337 Wb and $\lambda_i$=–0.0552885 Wb, respectively. The voltage drop across the low-voltage winding is then computed by

$$\vec{V} = -2\pi\times 60\times -0.0552885 + j2\pi\times 60\times 0.0989337, \tag{D.4}$$

and the calculation leads to

$$\vec{V} = 20.8433 + j37.2971 \text{ V}, \tag{D.5}$$

exactly the same voltage drop indicated in the third line of Table 2. In polar coordinates, the voltage drop is

$$\vec{V} = 42.75\angle 60.7^\circ \text{ V}. \tag{D.6}$$

Let $\boldsymbol{\lambda}_{\text{LV}}$ and $\boldsymbol{V}_{\text{LV}}$ denote the phasors associated to the flux linkage and voltage drop across the low-voltage winding, respectively. These two phasors are computed from the magnitudes $\|\boldsymbol{\lambda}\|$ and $\|\boldsymbol{V}\|$ using the following equations:

$$\vec{\lambda}_{LV} = \frac{\|\vec{\lambda}\|}{\sqrt{2}}\angle -29.3^\circ \text{ Wb} \tag{D.7}$$

and

$$\vec{V}_{LV} = \frac{\|V\|}{\sqrt{2}}\angle 60.7^\circ \text{ V}, \tag{D.8}$$

respectively.

**Voltage drop in the high-voltage winding**

Let $\boldsymbol{\lambda}$ denote the rotating vector associated to the flux linkage with the high-voltage winding. The voltage drop $\boldsymbol{V}$ across the high-voltage winding can be calculated by

$$\vec{V} = -\omega\lambda_i + j\omega\lambda_r. \tag{D.9}$$

Substitution of the numeric values indicated in Table 3 on the right-hand side of (D.9) gives

$$\vec{V} = -2\times\pi\times 60\times 0.405449 + j2\times\pi\times 60\times -0.725436, \tag{D.10}$$

and the calculation leads to the same voltage drop indicated in the third line of Table 3**,**

$$\vec{V} = -152.851 - j273.483 \text{ V}. \tag{D.11}$$

The graphical relationship between voltage drop and flux linkage in the two windings of the test transformer is illustrated in the vector diagram of Figure D-1.

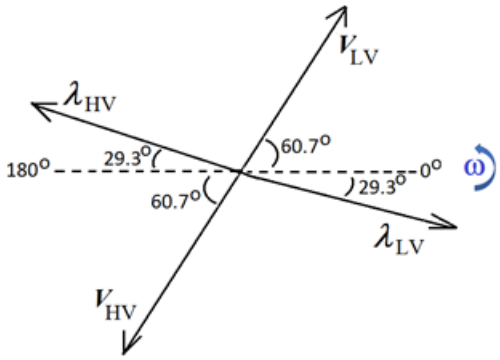


*Figure D-1. Phasor diagram relating voltage drop and flux linkage in the two windings.*

**Appendix E: Effect of the maximum hysteresis angle on global quantities**

To investigate the effect of the maximum hysteresis angle on global quantities like flux linkage, real power and reactive power, a sequence of similar problems with increasing values of the specified maximum hysteresis angle has been employed. All simulated problems refer to test transformer's no-load operation with a driving current $\boldsymbol{I}$=123 mA. The material properties of the laminated core are those indicated in the block scheme of Figure 4, but each problem concerns one specific configuration of the laminated core, characterized by the maximum hysteresis angle $\phi_{\text{hmax}}$. In the sequence of test problems, the maximum hysteresis angle varies in the range $0°\leq\phi_{\text{hmax}}\leq 30°$ in steps of 5°. Results of the simulations are presented in the graphs of Figure E-1 and Figure E-2 together with Table E-1.

*Table E-1: Variation of global quantities with respect to the maximum hysteresis angle.*

| **Max. Hyst. angle (degree)** | **0** | **5** | **10** | **15** | **20** | **25** | **30** |
|---|---|---|---|---|---|---|---|
| **Phase lag of $\lambda$ (degree)** | -11.6 | -16.1 | -20.5 | -24.9 | -29.2 | -33.4 | -37.6 |
| **Stored energy (millijoule)** | 3.61790 | 3.49419 | 3.35544 | 3.20390 | 3.04151 | 2.86995 | 2.69061 |
| **Reactive power (VAr)** | 2.72844 | 2.63516 | 2.53054 | 2.41628 | 2.29384 | 2.16448 | 2.02926 |
| **Active power (W)** | 0.56448 | 0.76457 | 0.95134 | 1.12488 | 1.28543 | 1.43334 | 1.56900 |

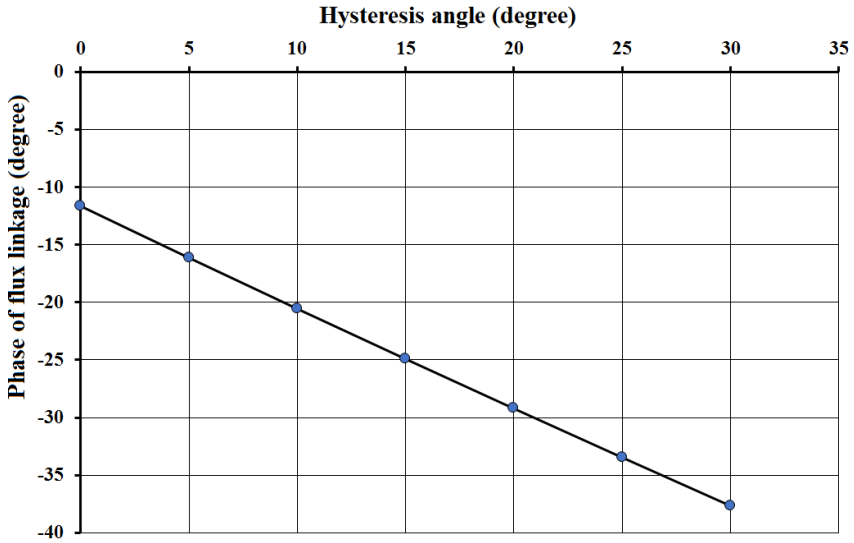


*Figure E-1. Variation of the phase lag of the flux linkage $\lambda$ with respect to the maximum hysteresis angle.*

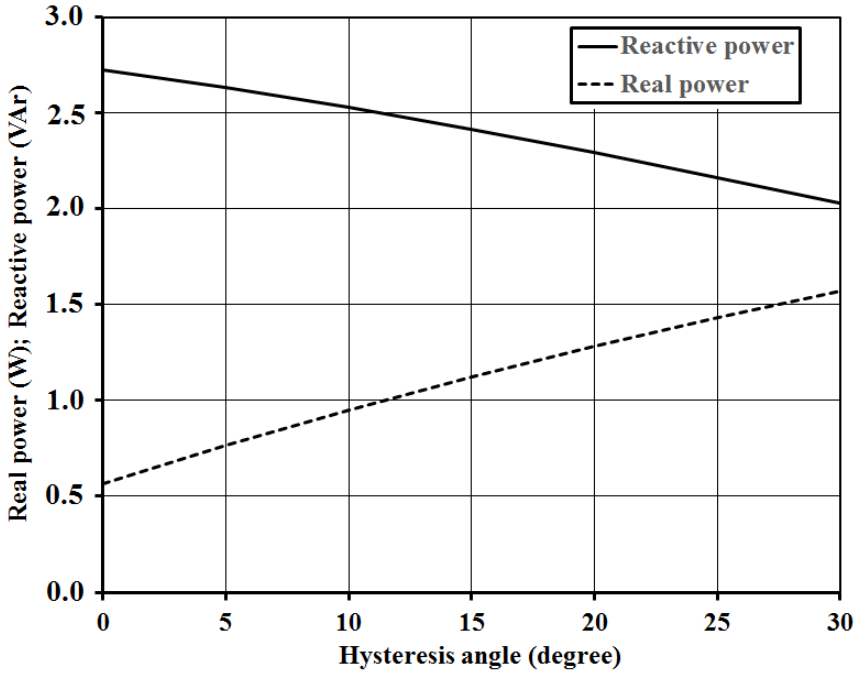


*Figure E-2. Variation of real and reactive power with respect to the maximum hysteresis angle.*

Observation of the graphs shown in Figure E-1 and Figure E-2 shows that, at this level of excitation, the changes in the core's permeability resulting from the increase in the maximum hysteresis angle alter all the global quantities related to the energizing winding, *viz*:

- The magnitude of the angle that represents the lag of flux linkage and complex inductance with respect to the driving current increases linearly, and this can be observed in the graph of Figure E-1;
- The real or active power *P* drawn from the supply increases almost three times, and this is caused by the increase in magnetic losses;
- The flow of reactive power *Q* decreases, and this is caused by the decrease in the core's magnetic energy storage. A simple calculation based on the values at the end-points of the simulated excursion shows that

$$W_m(30^\circ) \Big/ W_m(0^\circ) = Q(30^\circ) \Big/ Q(0^\circ) = 0.744 \text{ p.u.} \tag{E.1}$$

- The calculation presented in (E.1) shows that, along the simulated excursion, both the magnetic stored energy $W_m$ and the reactive power $Q$ undergo exactly the same decrease of 25.6%.
- The overall power consumption decreases. Given the intrinsic inductive nature of the "load", the variation in apparent power $|S|$ is strongly affect by the decrease in reactive power.

**Appendix F**: **Circuits with frequency-dependent elements: selected applications**

The electric circuit shown in Figure 6 contains the frequency-dependent lumped elements that represent the ohmic loss and magnetic stored energy related to the cored winding of the test transformer operating at no-load at the frequency of 60 Hz. Two elementary applications of this circuit are presented in the following.

**Kirchhoff's law and terminal voltage**

Application of Kirchhoff's law of voltages to the circuit of Figure 6 leads to

$$\vec{V}_s - \omega L_i \vec{I}_s - j\omega L_r \vec{I}_s = 0. \tag{F.1}$$

The terminal voltage, $\boldsymbol{V}_s$, can then be calculated by the vector addition

$$\vec{V}_s = \omega L_i \vec{I}_s + j\omega L_r \vec{I}_s. \tag{F.2}$$

Substitution of numerical values gives

$$\vec{V}_s = 20.84 + j37.30 \text{ V}, \tag{F.3}$$

practically the same terminal voltage indicated in **Table 2**. The vector addition expressed in (F.2) is illustrated in Figure F-1.

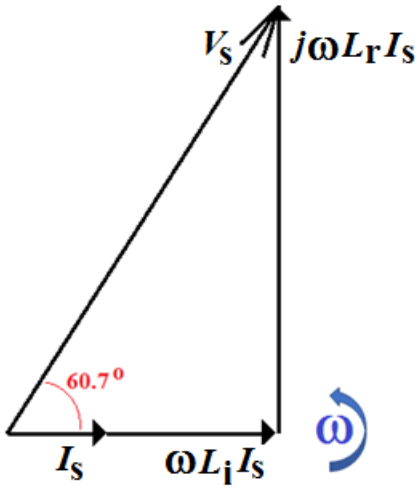


*Figure F-1. Graphical calculation of terminal voltage.*

**Computation of complex power**

Let $\boldsymbol{I}$ and $\boldsymbol{V}$ denote the phasor quantities associated to the winding's terminal current and terminal voltage, respectively. The magnitudes of both phasors are expressed in "rms" values. The complex power $S$ can be computed by using its definition,

$$S = \vec{V}\left(\vec{I}\right)^* = \frac{42.754}{\sqrt{2}}\angle 60.7^\circ \frac{0.123}{\sqrt{2}}\angle 0^\circ, \tag{F.4}$$

and this leads to

$$S = P + jQ = 1.285 + j2.294 \text{ VA}, \tag{F.5}$$

practically the same value of complex power indicated in the 6th line of Table 2.

In the other method of calculation, the computation of $P$ and $Q$ is based on the values of the resistive and inductive elements of the electric circuit of Figure 6. The averaged real power $P$ is computed by

$$P = \left(\omega L_i\right) I^2 = 1.285 \text{ W}, \tag{F.6}$$

and the reactive power $Q$ is computed by

$$Q = \left(\omega L_r\right) I^2 = 2.294 \text{ VAr}. \tag{F.7}$$